Analysis of the interaction between moving α/γ interfaces and interphase precipitated carbides during cyclic phase transformations in a Nb-containing Fe-C-Mn alloy

Dong, Haokai; Chen, Hao; Wang, Wei; Zhang, Yongjie; Miyamoto, Goro; Furuhara, Tadashi; Zhang, Chi; Yang, Zhigang; van der Zwaag, Sybrand

DOI
10.1016/j.actamat.2018.07.052

Publication date
2018

Document Version
Final published version

Published in
Acta Materialia

Acta Materialia 158 (2018) 167–179

Contents lists available at ScienceDirect

Acta Materialia

journal homepage: www.elsevier.com/locate/actamat

Full length article

Analysis of the interaction between moving α/γ interfaces and interphase precipitated carbides during cyclic phase transformations in a Nb-containing Fe-C-Mn alloy

Haokai Dong [a], Hao Chen [a, *], Wei Wang [b], Yongjie Zhang [c], Goro Miyamoto [c], Tadashi Furuhara [c], Chi Zhang [a], Zhigang Yang [a], Sybrand van der Zwaag [a, d]

[a] Key Laboratory of Advanced Materials of Ministry of Education, School of Materials Science and Engineering, Tsinghua University, Beijing, 100084, China
[b] Department of Hot Rolled Strip, Baosteel Research Institute, Shanghai, 201900, China
[c] Institute for Materials Research, Tohoku University, Aoba-ku, Sendai, Miyagi, 980-8577, Japan
[d] Faculty of Aerospace Engineering. Delft University of Technology, Delft, the Netherlands

ARTICLE INFO

Article history:
Received 10 May 2018
Received in revised form
18 July 2018
Accepted 22 July 2018
Available online 24 July 2018

Keywords:
Phase transformation
Interphase precipitation
Carbide
Pinning force
Interface migration

ABSTRACT

The interaction between moving α/γ interfaces and interphase precipitated (IPd) carbides during the austenite (γ) to ferrite (α) and the ferrite (α) to austenite (γ) transformation has been systematically investigated through cyclic phase transformation experiments for a 0.1C-1.5Mn alloy containing 0.1 wt% Niobium (Nb) and its Nb-free counterpart. Shifts in the critical reaction temperatures during continuous heating and cooling are observed, which are attributed to the pinning force (PF) originating from the IPd carbides present. By applying the Gibbs energy balance (GEB) model to analyze experimental results, the PF was derived to be about 15 J/mol for the α→γ transformation and about 5 J/mol for the γ→α transformation, respectively, both of which are quite small compared to chemical driving force of phase transformations. Moreover, various modified Zener pinning equations have also been used to predict the PF, and it was found that these values are comparable with those obtained from experiments, which suggests that the classical Zener theory still has promising potential for carbide-interface interaction analysis.

1. Introduction

The autonomous formation of dispersed nanosized second-phase particles at moving grain boundaries has been recognized as an important means to inhibit grain growth and to achieve better mechanical properties in metallic materials [1]. Extensive kinetics studies have been conducted to quantitatively estimate the pinning force (PF) [2–8] on moving grain boundaries during recrystallization and there seems to be a convergence regarding the nature and strength of the actual pinning process. However, the issue of the PF of such particles on the moving austenite-ferrite interfaces is more complex than during recrystallization because of the locally varying chemical composition of the moving interface and the local transition in crystal structure.

Interphase precipitation (IP) is a special phenomenon in micro-alloyed steels that originates from the periodic nucleation of carbides around the moving α/γ interface [9,10], resulting in the appearance of highly organized carbide arrays on specific crystallographic planes. Due to its regular arrangement along the interphase boundary, interphase precipitated (IPd) carbides can be used as a suitable model phase to study the particle-interface interaction. However, given the close correlation between mechanical properties and microstructure of IP, most previous studies focused on the clarification of carbide size and inter-sheet spacing dependence on the transformation temperatures during the austenite-ferrite (γ→α) transformation [10–15]. Considerably less attention has been paid to the interaction between the presence of IPd carbides and the motion of the α/γ interface as such (i.e. both for the γ→α and the α→γ transformation).

Moreover, identification of PF from carbide arrays is also crucial for elucidating the physical mechanisms of IP, which has been considered in several models but still remains controversial. One group [16–19] argues that PF is large and plays a significant role during IP. Ricks and Howell [16,17] presented experimental results

* Corresponding author.
E-mail address: hao.chen@mail.tsinghua.edu.cn (H. Chen).

https://doi.org/10.1016/j.actamat.2018.07.052
1359-6454/

of α/γ interfaces being pinned by $M_{23}C_6$ precipitates in an Fe-10Cr-0.2C alloy and proposed a bowing mechanism to account for it. They used an energy balance criterion to model the bowing process and showed that there exists a critical particle spacing below which the bowing mechanism is energetically unfavourable. Liu [18] attributed the formation of parallel sheet particles to the relative variations of the driving force and PF exerted on the moving α/γ interfaces during the austenite decomposition. The maximum amount of PF obtained from Liu's model is about 24 MPa (~326 J/mol). Chen et al. [19] proposed a super-ledge model to predict the evolution of IP, in which the lateral motion of ledge will be pinned by IPd carbides unless the height of ledge reaches a critical value to surmount PF. While another group [20–22] suggests that PF is quite small in comparison with the chemical driving force and thus can be ignored. Murakami et al. [20] used the classical Zener pinning equation modified by Gladman [3] to estimate the PF, and found its value to be about 6 J/mol. The Zener's equation has been derived based on several simplifying assumptions [7]: (1) all particles are spherical and of equal size, (2) the particles are incoherent with matrix, (3) the particles are randomly distributed. Obviously, these simplifications do not apply to particles as formed during IP. Mukherjee et al. [21,22] pointed out that both nanoclusters and nano-precipitates could be observed by atom probe microscopy in Ti-Mo microalloyed steels after thermomechanical processing. The fact that large fractions of disc-shaped nanoclusters and precipitates remain coherent or semicoherent with the ferrite matrix indicates a negligible interfacial energy between two phases, which may exert a marginal pinning effect upon the moving α/γ interfaces.

In order to investigate the carbide-interface interaction, the cyclic phase transformation concept, which was initially designed to study the growth kinetics of partitioning (γ→α and α→γ) phase transformations in the absence of concurrent nucleation processes [23,24], has been applied in the present work. By applying the Gibbs energy balance (GEB) model, the PF from IPd carbides acting on migrating interfaces both for the austenite to ferrite and the ferrite to austenite transformation is quantitatively determined. The accuracy of the values of PF and its dependence on phase transformation directions are discussed. A comparison between the derived PF and those calculated via different Zener pining equations is also made.

2. Experimental methods

2.1. Experimental design

Two alloys, Fe-0.1C-1.5Mn and its Nb containing equivalent Fe-0.1C-1.5Mn-0.1Nb were used in the present study. For simplicity, they are designated as 0Nb and 0.1Nb alloys hereafter. Before describing in detail the experimental conditions imposed (section 2.2) and the model used to guide the selection of the thermal route (section 3.1), let us first explain the concept underlying the experiment.

As shown in Fig. 1a, the actual analysis starts with a fully austenitized sample being isothermally held at an intercritical temperature T_1 for a certain time to obtain a mixed ferrite–austenite microstructure (Process I). In the 0.1Nb alloy, this leads to the formation of rows of IPd carbides in the ferrite while such is not the case in the 0Nb alloy. The samples are then continuously reheated to the second intercritical temperature T_2 which is higher than the critical NPLE/PLE $\alpha\rightarrow\gamma$ temperature ($PNTT_{\alpha\rightarrow\gamma}$) and the samples are held there isothermally, which make the interface move back into the ferrite phase (Process II). The highly organized carbide arrays located in the ferrite will induce a PF and hinder the interface advancement in the 0.1Nb alloy. No such particle obstacles are present in the 0Nb alloy and this results in a higher interface velocity. After an isothermal hold at T_2, the samples are cooled linearly to T_3 which is lower than the critical NPLE/PLE $\gamma\rightarrow\alpha$ temperature ($PNTT_{\gamma\rightarrow\alpha}$) and the cooling is followed by isothermally holding. This thermal treatment makes the interface again move forward into the newly formed austenite (Process III). For the 0.1Nb alloy, PF will be generated again between the moving interface and IPd carbides retained in the new austenite. No such interactions are present in the 0Nb alloy and its passage is uninterrupted. The microstructural evolution during the I, II and III processes are also schematically shown in Fig. 1b. Moreover, to be successful in determining the actual PF, it is important that the initial driving force for $\alpha\rightarrow\gamma$ and $\gamma\rightarrow\alpha$ phase transformation of two alloys should be kept the same or at least quite comparable. For the carbon diffusion-controlled reaction, the amount of driving force heavily depends on the carbon enrichment in austenite, which follows from the volume fraction of proeutectoid ferrite and austenite. These fractions can be determined from the dilatometric signal (application of the lever rule) or by quantitative metallurgy through appropriate quenching. It is worth noting that in this work, the total amount of carbon consumed by the NbC formation can be reasonably neglected, e.g. 0.1mass% Nb consumes at most ~0.01mass% C against the bulk 0.1mass% C, in the carbon analysis of the austenite ↔ ferrite transformation.

2.2. Experimental procedure

The as-received hot rolled alloys were firstly cut into blocks of $100 \times 25 \times 12 mm^3$ and then encapsulated into a silica tube filled with pure Ar gas for homogenization at 1523 K for 21.6ks. Chemical compositions of the alloys after homogenization and their characteristic temperatures are listed in Table 1. The homogenized blocks were machined into standard cylindrical samples (4 mm in diameter and 10 mm in length) for dilatometry experiments.

Based on the experimental approach outlined above and a large number of exploratory experiments, the critical temperatures T_1, T_2 and T_3 and three cyclic partial transformation routes plotted in Fig. 2 were determined. The γ/(α+γ) phase boundaries under the LE condition for both alloys shown in Fig. 2a were obtained by the same calculation method as used in Ref. [25]. The Nb addition has marginal effects on the location of NPLE/PLE lines so the same lines as for the Nb-free material. In order to create the same carbon content in the initially formed intercritical austenite, the 0Nb samples were isothermally held at 700 °C for 30min after austenitization, while the 0.1Nb samples were held for 40min. To induce the $\alpha\rightarrow\gamma$ transformation, both alloys were then heated linearly to 800 °C followed by quenching, which is called a type I1 experiment as shown in Fig. 2b. Likewise, for the $\gamma\rightarrow\alpha$ transformation, both alloys were heated to 790 °C followed by isothermal holding for 20min in aim to obtain the same carbon concentration in austenite, then continuously cooled to 680 °C followed by quenching, which is called a type H1 experiment as shown in Fig. 2c. In order to study the PF effects on the isothermal transformation kinetics, a type H2 experiment was also conducted as indicated in Fig. 2d, among which the dashed lines represent the interrupted quenching process for the microstructural observation after each cycle. A heating (or cooling) rate of 5 °C/s in type H1 and H2 experiments is used to have comparable kinetics for both alloys. The austenitizing temperature of 1250 °C was chosen to dissolve all the NbC. All thermodynamic data for the two alloys used in this study are calculated using Thermo-Calc with the TCFE7 database.

A Bahr DIL805A/D dilatometer equipped with a laser diameter detector was used for the thermal treatment. Kinetics of cyclic phase transformation could be derived from the dilatation curves. Transformed specimens were polished and etched with 4% Nital

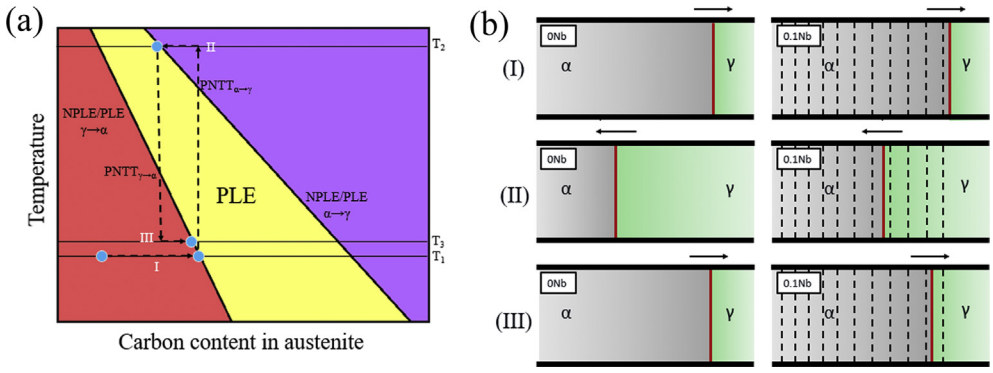

Fig. 1. Schematic diagram showing (a) the route of cyclic phase transformations guided by the map of LE model and (b) corresponding microstructural evolution to study the interaction between moving α/γ interface and IPd carbides. NPLE/PLE line is the boundary for the transition from NPLE mode into PLE mode.

Table 1
Chemical compositions and characteristic temperatures for the two alloys.

Alloy	Composition (mass%)					Temperature (^{0}C)		
	C	Mn	Si	Nb	Fe	Para-Ae3	PLE/NPLE	Solution temp. of NbC in γ
0Nb	0.1	1.5	0.05	–	Bal.	807	763	–
0.1Nb	0.077	1.5	0.05	0.1	Bal.	811	765	1186

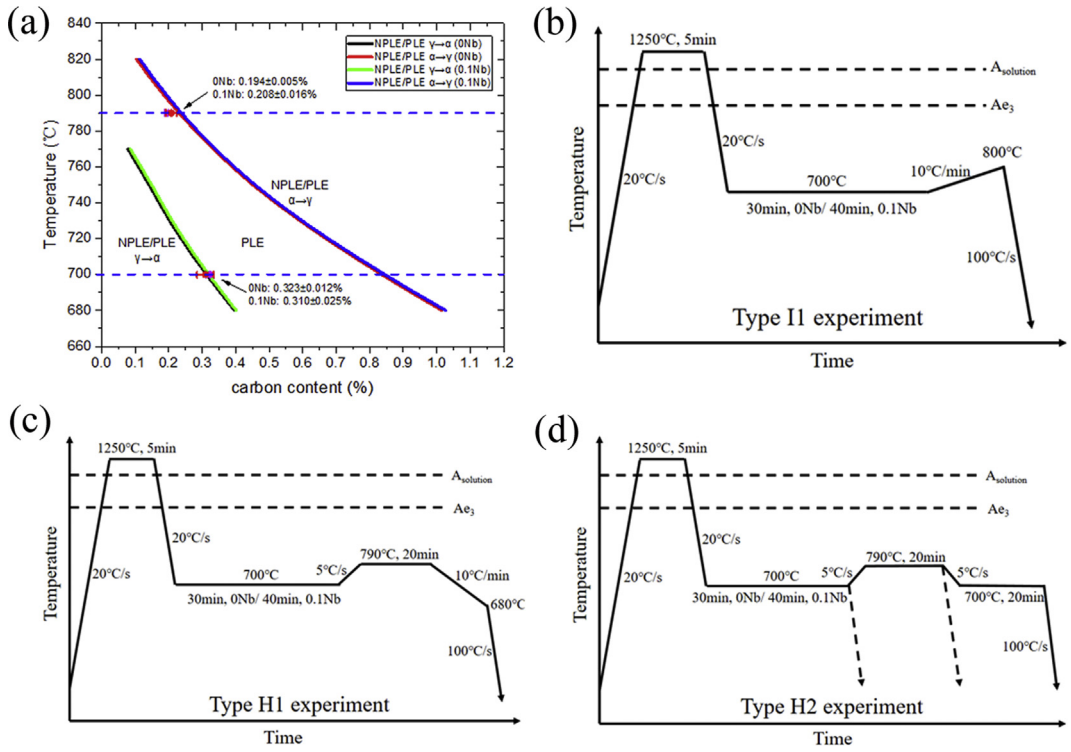

Fig. 2. (a) γ/(α+γ) phase boundaries under the LE conditions for both alloys. The heat treatment for (b) type I1, (c) type H1 and (d) type H2 cyclic experiments. The dashed lines in (d) mark the interrupted quenching process in order to determine the microstructures after each segment of the cycle. Red and purple solid circles in (a) indicate the average carbon enrichment in austenite after each interrupted quenching process in (d) for 0.1Nb and 0Nb alloys, respectively. (For interpretation of the references to colour in this figure legend, the reader is referred to the Web version of this article.)

solution for optical microscopy. Volume fractions of ferrite were quantified by point counting method using at least 8 OM images at the magnification of 100, and converted into the average carbon content in austenite by the level rule. For characterisation of the carbide formed by IP, transmission electron microscopy (TEM; FEI Tecnai G20 operated at 300 kV) was carried out. The TEM samples were produced by cutting slices from the dilatometry specimens and were mechanically thinned to 50 μm on SiC papers. Then the thin-foil specimens were twin-jet electropolished at 20 V in a solution of 10% perchloric acid and 90% ethanol at −30 °C. The 3DAP measurements (CAMECA LEAP-4000 HR), whose specimens were prepared through focused ion beam (FIB; FEI Quanta 3D) microsampling method, were subsequently performed at 50 K with 20% for pulse fraction and 200 kHz for pulse rate to observe the possible precipitation of alloy carbide and segregation of alloying elements at the migrating α/γ interface. After reconstruction of the raw data

on the IVAS ver. 3.6 software by using the SEM images taken in advance, the correction of detection loss of Fe ions was carried out to obtain more accurate alloy contents [26].

3. Models

The Local equilibrium (LE) model and GEB model have been adopted to quantitatively analyze the interaction between IPd carbides and the moving α/γ interface during the cyclic phase transformations. It needs to be emphasized that the LE condition has been demonstrated to be a special case of the GEB model, which is thoroughly discussed in Ref. [27].

3.1. Local equilibrium model

Depending on the partitioning behaviour of the substitutional elements M, the LE model distinguishes two modes [28,29]. One is called negligible-partition local equilibrium (NPLE) mode. In this mode, the transformation rate is fast and controlled by C diffusion, while M does not redistribute, but form a concentration spike just ahead of the α/γ interface. The other one is called partition local equilibrium (PLE) mode, in which both M and C atoms partition between ferrite and austenite leading to a slower transformation kinetics because of the slow Mn diffusion involved.

3.2. Gibbs energy balance model

3.2.1. Chemical driving force

From a thermodynamics viewpoint, the chemical driving force for a phase transformation is essentially determined by the chemical potential difference for each alloying element on both sides of the interface, which can be calculated as:

$$\Delta G_m^{chem} = \sum_i^n x_i^0 \left[\mu_i^{\gamma/\alpha}\left(x_i^{\gamma/\alpha}\right) - \mu_i^{\alpha/\gamma}\left(x_i^{\alpha/\gamma}\right)\right] \tag{1}$$

Where x_i^0 is the concentration of the element i transferred over the interface, n is the number of elements, $x_i^{\gamma/\alpha}$ and $x_i^{\alpha/\gamma}$ are the mole fractions of the element i at the interface on the austenite and ferrite side, respectively. $\mu_i^{\gamma/\alpha}$ and $\mu_i^{\alpha/\gamma}$ are the chemical potential of i in ferrite and austenite. For the non-partitioning $\alpha \rightarrow \gamma$ transformation, the chemical driving force can also be calculated in the similar way as long as the composition of the parent and new phase are known.

In general, the growing kinetics of grain boundary ferrite can be adequately analysed by a one-dimensional growth model. The C diffusion controlled transformation can be divided into two stages [30]: (i) the non-overlapping diffusion stage, in which diffusion fields ahead of opposing interfaces in the parent phase do not overlap; (ii) the overlapping diffusion stage or soft impingement stage, in which the diffusion field starts to overlap and slow down the reaction.

Combining the mass conservation and diffusion equations, the interface velocity v and diffusion field length L at the non-overlapping stage are derived by the following equation [30]:

$$v = \frac{2D_C^{\gamma}\left(x_C^{\gamma/\alpha} - x_C^0\right)}{L\left(x_C^{\gamma/\alpha} - x_C^{\alpha/\gamma}\right)} \tag{2}$$

$$L = \frac{3S\left(x_C^0 - x_C^{\alpha/\gamma}\right)}{\left(x_C^{\gamma/\alpha} - x_C^0\right)} \tag{3}$$

Where S is the thickness of new phase, D_C^{γ} is the diffusion coefficient of C in austenite, $x_C^{\gamma/\alpha}$ is the mole fraction of C at the interface in austenite, $x_C^{\alpha/\gamma}$ is the mole fraction at the interface in ferrite, x_C^0 is the mole fraction of C in the austenite.

For the overlapping stage, the interface velocity v and the C concentration in the middle of austenite can be expressed as [30]:

$$v = \frac{2D_C^{\gamma}\left(x_C^{\gamma/\alpha} - x_C^m\right)}{L\left(x_C^{\gamma/\alpha} - x_C^{\alpha/\gamma}\right)} \tag{4}$$

$$x_C^m = \frac{3S\left(x_C^0 - x_C^{\alpha/\gamma}\right)/L + 3x_C^0 - x_C^{\gamma/\alpha}}{2} \tag{5}$$

$$L = L_0 - S \tag{6}$$

Where x_C^m is the carbon concentration at the center of the austenite and L_0 is the half thickness of austenite.

As for the partial cyclic transformations, C diffusion field will appear in both austenite and ferrite phase. However, due to the very high diffusivity of C in ferrite compared to that in austenite, C gradient in ferrite can be negligible, thus interface migration is still controlled by C diffusion in austenite regardless of transformation directions. The kinetics of ferrite growth or austenite growth during the cyclic transformations can be also described as equations (2)–(6) once the initial C content in both phases are identified.

Coupling Eqs. (1), (2) and (4), the chemical driving force can be calculated as a function of the interface velocity v and the thickness of the new phase S.

3.2.2. Dissipation of Gibbs energy

Generally, the Gibbs energy dissipation in a moving α/γ interface is due to two processes: (i) dissipation due to solutes diffusion inside the interface, which is so-called solute drag effect (SDE); (ii) dissipation due to atom rearrangement across interface, which is the so-called intrinsic friction.

During diffusional phase transformations, the substitutional alloying elements tend to segregate at the migrating interfaces due to the potential well inside interfaces, which in the present work is regarded as a triangular configuration originally proposed by Purdy and Bréchet. In Fig. 3, the schematics of the potential well for austenite stabilizer (e.g. Mn, Ni, etc.) is shown. μ_α^0 and μ_γ^0 are the chemical potential of the solute in the ferrite and austenite, respectively; E_0 is the binding energy; ΔE is the half of the solute chemical potential difference between austenite and ferrite, and its value depends on the partition coefficient of the solutes and temperature. δ is the half thickness of the interface.

By solving the governing equation for solute diffusion [31], the solute profile inside the interface at any given velocity can be constructed. The dissipation due to solute drag effect can be derived from Cahn's equation [19]:

$$\Delta G_m^{SDE} = PV_m = -\int_{-\delta}^{+\delta} (X - X_0)\left(\frac{dE}{dx}\right)dx \tag{7}$$

where P is the solute drag force, which results from the asymmetric solute distribution inside the interface, V_m is the molar volume, and X_0 is the bulk concentration of solutes in the alloys. It needs to be noted that the solute profile inside interface not only depends on the interface velocity but also on the direction of migrating as shown in Fig. 3, which in turn can affect the amount of energy dissipation.

The energy dissipation due to interface friction can be written as:

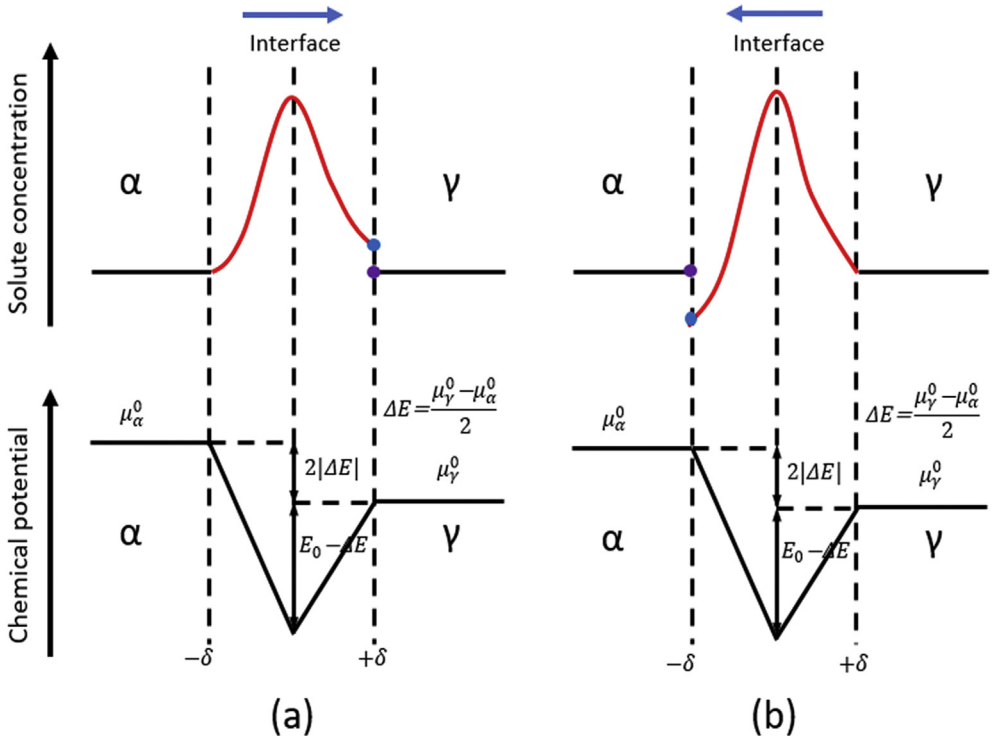

Fig. 3. The schematics of austenite stabilizer's profile and potential well inside the interface for (a) γ→α transformation and (b) α→γ transformation.

$$\Delta G_m^{friction} = vV_m/M_{\text{int}} \tag{8}$$

Where M_{int} is the intrinsic interface mobility, and its value is set to 0.035exp(-147000/RT) $m^4/J\,s$ as suggested by Hillert [32].

It should be emphasized that in this work, due to the interaction between moving interfaces and carbide arrays, an additional dissipation term due to PF (ΔG_m^{PF}) has to be considered. For simplicity of analysis, and because we have no physical arguments to postulate a certain dependence of PF on interface velocity or temperature for the conditions explored, we assume PF to be constant.

3.2.3. Gibbs energy balance

So far, both the chemical driving force and the total dissipation can be calculated as a function of the interface velocity. According to the core concept of GEB model, the driving force should be equal to the dissipation of Gibbs energy:

$$\Delta G_m^{chem}(v) = \Delta G_m^{SDE}(v) + \Delta G_m^{friction}(v) + \Delta G_m^{PF} \tag{9}$$

By solving eq. (9) numerically, the growth rate of new phase for quasi-steady state can be obtained.

4. Results and discussion

4.1. Experimental results

4.1.1. Microstructures

Fig. 4(a–d) shows the microstructures of 0Nb and 0.1Nb specimens treated to the interrupted quenching process as described in type H2 experiment. The figure proves significant growth of austenite in both alloys during isothermal holding at 790 °C and there are no signs of additional nucleation of austenite, i.e. the growth of austenite is realised by the migration of interfaces existing at the end of the first isothermal treatment at 700 °C. The average carbon enrichment in austenite based on proeutectoid ferrite fractions determined using the lever rule method has been marked in Fig. 2c and is listed in Table 2. Fig. 4e-f shows TEM micrograph of IP obtained from the ferrite phase of the 0.1Nb specimen having received the same treatment as Fig. 4b and the corresponding diffractogram, which confirms that the precipitation behaviour of the carbides proceeded via the formation of planar IP. Typical features of IP are also determined: (1) the plane containing the rows of precipitates is close to $(-110)_\alpha$, (2) the average inter-sheet spacing is ~20 nm, (3) the average diameter of NbC is 6 ± 1.5 nm, based on the data obtained from more than 70 carbides in different ferrite grains.

In order to illustrate the redistribution of alloying elements and the presence of carbides after the cyclic process, 3DAP measurements are conducted on the 0.1Nb specimen having received the same treatment as the sample shown in Fig. 4d. Fig. 5(a–c) are the three-dimensional atom maps of C, Nb and Mn, respectively, focussing on a cylindrical region of interest with a diameter of 30 nm as shown in Fig. 5d, to exhibit their corresponding one-dimensional concentration profile across the α/M(γ) interface in Fig. 5e. Both C and Mn are remarkably segregated at the α/M(γ) interface. A slightly partitioning of Mn due to the high temperature cycle is also observed between two phases, but the diffusion distance at 790 °C evaluated by $\sqrt{D_{Mn}^{\gamma}t}$ (D_{Mn}^{γ} is the diffusion coefficient of Mn in austenite, t is the isothermal holding time) is only ~ 27 nm, which means Mn redistributes just near the interface and no bulk partitioning occurs. Interestingly, two NbC particles with similar size are apparently situated on both sides of the interface, which provides a direct evidence that the interfaces move back and carbides are retained in newly formed austenite, as schematically shown in Fig. 1b(II). What's more, the fact that no local enrichment of Nb around the α/M(γ) interface is observed indicates that the original bulk Nb has been consumed by IP during the previous γ→α transformation.

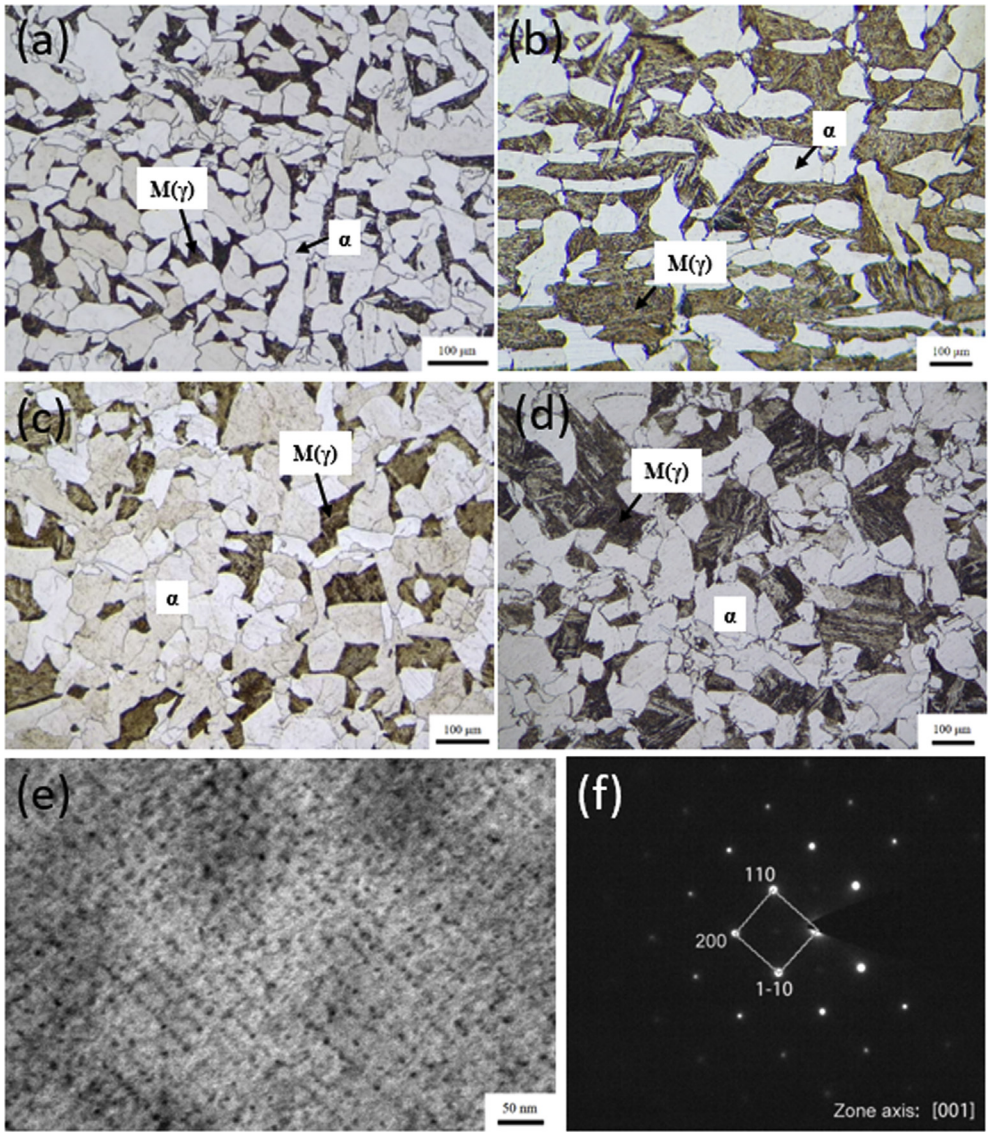

Fig. 4. Optical micrographs showing microstructures of (a, b) 0Nb and (c, d) 0.1Nb specimens isothermally treated at 700 °C (process I) for 30min (a) and for 40min (c), followed by 20min isothermally holding at 790 °C (process II) for 0Nb (b) and 0.1Nb (d); TEM image of IP (e) obtained from the ferrite constituent of 0.1Nb specimen as shown in (c) and the corresponding diffractogram (f). α: ferrite, M(γ): martensite transformed from untransformed austenite during quenching.

Table 2
Calculated carbon content in untransformed austenite based on proeutectoid ferrite fractions using level rule for 0Nb and 0.1Nb samples with different heat treatments.

Heat treatment	Sample			
	0Nb		0.1Nb	
	Measured ferrite fraction	Calculated carbon content in γ	Measured ferrite fraction	Calculated carbon content in γ
Process I (700 °C)	69.04 ± 1.03%	0.323 ± 0.012%	75.15 ± 1.85%	0.310 ± 0.025%
Process II (790 °C)	48.45 ± 1.12%	0.194 ± 0.005%	62.98 ± 2.64%	0.208 ± 0.016%

4.1.2. Interaction between α/γ interface and IPd carbides during the α→γ transformation

Fig. 6 shows the partial dilatation curves of type I1 experiments for the 0Nb and 0.1Nb alloys, respectively. It suggests that the process of the heating cycle can be divided into two stages: (i) a stagnant stage (A_1-A_2) derived from the approximately linear expansion curve, during which no phase transformation or interface migration occurs. (ii) a contraction stage (A_2-A_3) due to the α→γ transformation, during which the interface is moving back into the original ferrite phase. The abnormal expansion part (marked by the red dashed rectangle) during heating in both alloys is related to the magnetic transition, which has also appeared in pure iron near the Curie temperature and is thought to be caused by a change of electron–phonon interaction under the radio frequency field [33]. Moreover, as arrowed in Fig. 6a, the onset transformation temperature (Point A_2, 772 °C) for 0Nb specimen is basically consistent with the calculated transition temperature ($PNTT_{\alpha\rightarrow\gamma} = 771$ °C), while the behaviour for the 0.1Nb specimen

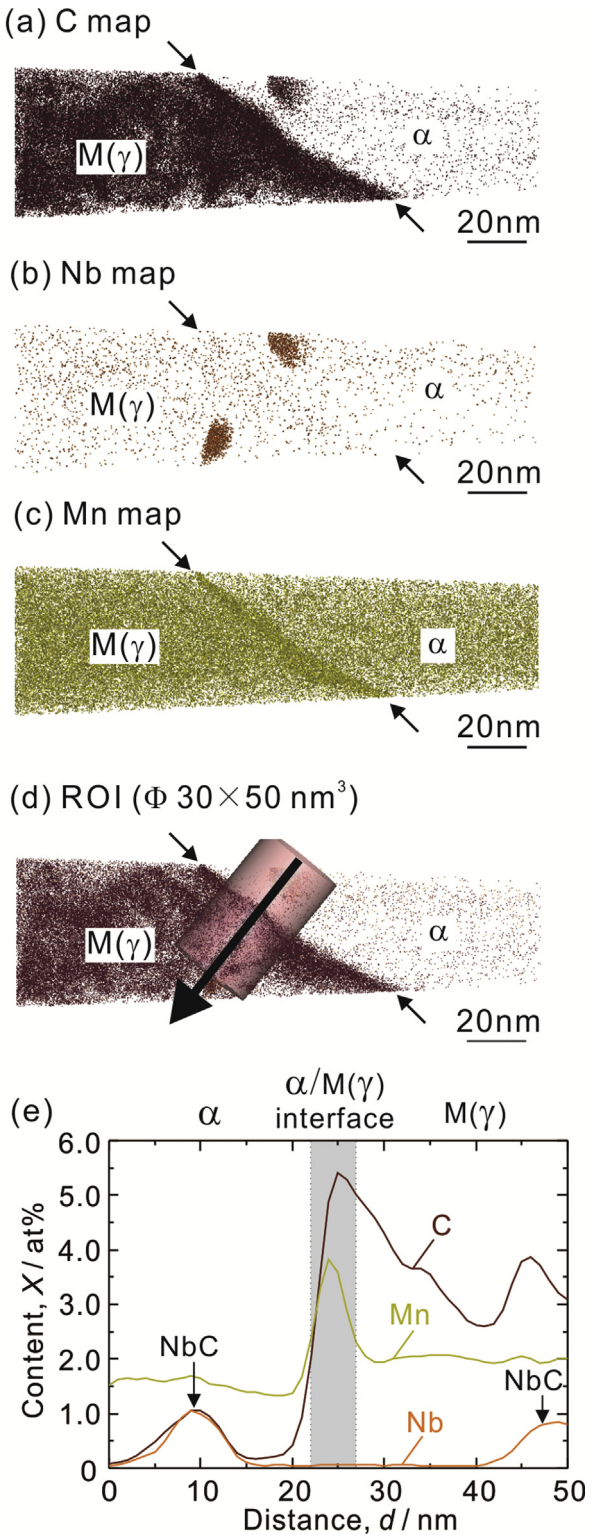

Fig. 5. Three-dimensional atom maps of (a) C, (b) Nb, (c) Mn, respectively, of the 0.1Nb specimen as shown in Fig. 4d, with (d) ROI of Φ 30 × 50 nm^3 and (e) corresponding one-dimensional C, Nb and Mn concentration profiles along bold arrow in (d), across α/M(γ) interface indicated by slim arrows in (a) ~ (d).

shown in Fig. 6b is different. The onset temperature of the transformation (783 °C) is delayed in comparison to the $PNTT_{\alpha\rightarrow\gamma}$ (776 °C). The temperature difference indicates that the back-migration of the interface is impeded by the IPd carbides present,

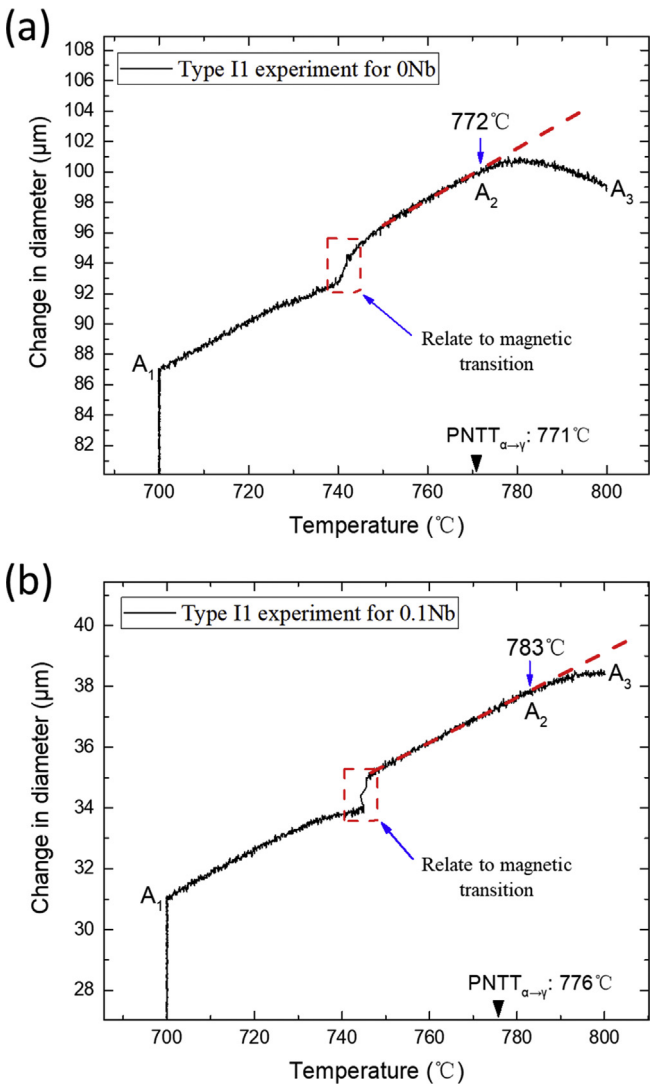

Fig. 6. The partial dilatation curves as a function of temperature for the (a) 0Nb and (b) 0.1Nb alloys during the type I1 experiment.

thus necessitating a higher temperature to obtain enough driving force for transformation initiation.

Now the GEB model combined with the experimental results is applied to quantitatively determine the PF. In the previous studies [27,34], the thickness of the interface 2δ is assumed to be 0.5 nm, and diffusion coefficient of the substitutional element M inside the interface D_M^{Int} is the geometric average of the diffusion coefficient of M in austenite (D_M^{FCC}), in ferrite (D_M^{BCC}) and in the ferrite grain boundary (D_M^{GB}). Values of each coefficient are obtained from Ref. [35]. The binding energy of Mn was chosen to be 9.9 kJ/mol, which is the same value as that used in Refs. [27,34].

Fig. 7a shows the calculated total dissipation, the dissipation due to SDE of Mn, dissipation due to Mn spike and dissipation due to interface friction, respectively, as a function of interface velocity for both alloys at 760 °C. When the interface velocity is very fast ($\geq 10^{-4}$ m/s), the dissipation due to SDE and due to spike are both small, while the intrinsic interface mobility starts to play a role. When the interface velocity is extremely low ($\leq 10^{-8}$ m/s), the values of SDE term and interface friction term approaches zero, and the total dissipation will be dominated by the spike term. Additionally, as described in Fig. 5e for the 0.1Nb alloy, Nb content in the transformed austenite (i.e. ferrite) is almost zero as a result of the

occurrence of IP. Hence, the total dissipation for the subsequent $\alpha \rightarrow \gamma$ transformation is thought to be caused mainly by Mn, which is the same as in the 0Nb alloy.

In Fig. 7b-c, the total energy dissipation in both alloys is plotted together with available chemical driving force at the initial stage ($S_\gamma = 0.1$ μm) for the $\alpha \rightarrow \gamma$ transformation at different temperatures. Fig. 7b shows that at 760 °C, the chemical driving force for the both alloys is lower than the dissipation at any interface velocity, which indicates the transformation kinetics is quite sluggish and it is controlled by the bulk diffusion of Mn in the ferrite. Hence this condition is located in the PLE region and coincident with the stagnant stage. With a further increase of temperature. e.g. 775 °C as shown in Fig. 7c, the chemical driving force of 0Nb alloy can overcome the dissipation caused by the Mn spike, thus the NPLE mode is operative which contributes to a relatively fast transformation rate. Whereas for the 0.1Nb alloy the transformation is still controlled by the PLE mode; thus almost no transformation happens. When the temperature rises to the 783 °C (Fig. 7d), the chemical driving force of both alloys can surmount their restraining forces. Hence, in theory, the $\alpha \rightarrow \gamma$ reaction for 0.1Nb alloy should occur at a measurable rate. However, as indicated by the dilation curves (Figs. 6b), 783 °C is just the starting transformation temperature, which means no obvious reaction takes place at this point. In other words, there exists an additional barrier, i.e. PF exerted by IPd carbides, resulting in the postponement of the back transformation. As mentioned in section 3.2.3, due to the uncertain relationship between the temperature and PF so far, the energy level related to PF is assumed to be temperature independent in a specific transformation direction. Therefore, at critical reaction temperature, the amount of PF should be physically equal to the difference between the chemical driving force and dissipation at zero interface velocity, which can be obtained about 15 J/mol as indicated in Fig. 7d and corresponds to 7 °C superheating in Fig. 6b. It needs to be explained that the Nb solute in transformed austenite might not be completely consumed, however, if assuming all the Nb atoms (0.1mass%) remain solute solution in the ferrite, the energy dissipation due to Nb present can be estimated to be very close to zero in case the interface velocity is very low ($\leq 10^{-8}$ m/s), as shown by green dashed line in Fig. 7d, thus leading to a negligible effect on PF determination.

Fig. 8 shows the fraction of austenite predicted by the GEB model and that measured experimentally as a function of time during the isothermal $\alpha \rightarrow \gamma$ transformation at 790 °C in the 0.1Nb alloy. The vertical axis symbols of $f_\gamma(t=0)$ and $f_\gamma(t)$ represent the austenite fraction at the initial stage and as a function of time during isothermal holding, respectively. By assuming different values of PF, the experimental transformation curve can be well fitted by the GEB model. The fitting process indicates that the PF may vary as a function of transformation degree but cannot be very large (e.g. 50 J/mol), just remains within the range of 0–10 J/mol, which is basically in agreement with the value obtained from the type I1 experiments.

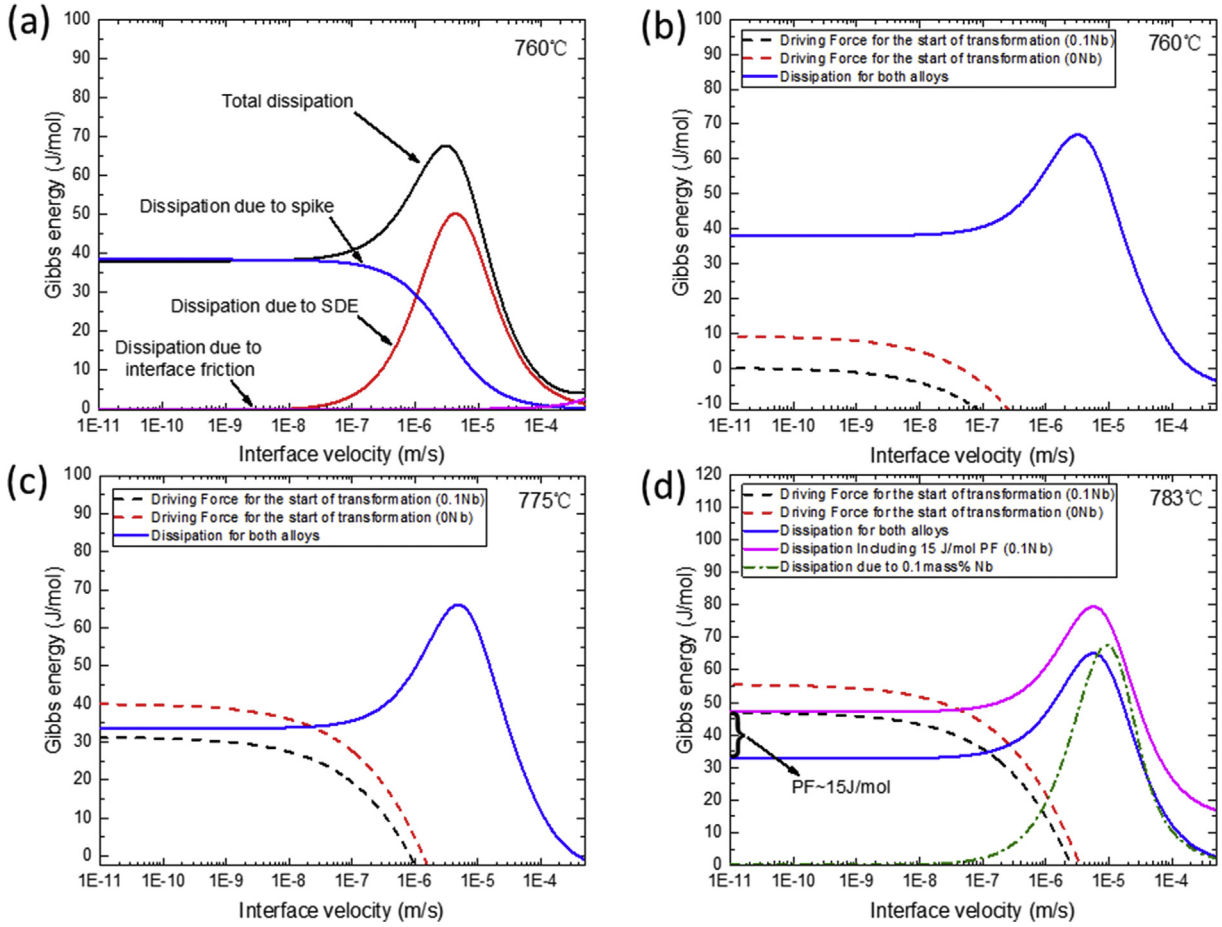

Fig. 7. (a) The total dissipation, dissipation due to SDE of Mn, dissipation due to Mn spike, dissipation due to interface friction as a function of interface velocity for both alloys at 760 °C. The total energy dissipation and available chemical driving force at the initial stage ($S_\gamma = 0.1$ μm) for the both alloys during the $\alpha \rightarrow \gamma$ transformation at (b) 760 °C, (c) 775 °C and (d) 783 °C, respectively.

4.1.3. Interaction between α/γ interface and IPd carbides during γ→α transformation

In Fig. 9, the partial dilatation curves as a function of temperature for both alloys during the type H1 experiment is shown. As for the α→γ transformation, the approximately linear dilation in the heating (B_1-B_2) and in the cooling (B_3-B_4) cycle can be considered as stagnant stage; for both alloys a distinctive contraction (B_2-B_3) is observed after the isothermal holding at 790 °C, during which the interface migrates back into the original ferrite. Again, the abnormal diameter change in both alloys during heating and cooling is deemed to be a variation of electron–phonon interaction during magnetic transition [33], though the variation degree of heating is smaller than that of cooling due to the faster heating rate (5 °C/s). Emphasis should be placed on the nonlinear expansion stage (B_4-B_5), which is attributed to the γ→α transformation. As indicated in Fig. 9a, the onset temperature of reaction for 0Nb alloy is 733 °C (Point B_4), which is basically in agreement with the $PNTT_{\gamma\to\alpha}$ (732 °C). The result for the 0.1Nb alloy shown in Fig. 9b, is quite similar. The measured onset temperature of reaction (729 °C) is quite close to the $PNTT_{\gamma\to\alpha}$ (731 °C), which means the pinning effect imposed by IPd carbides is insignificant when the interface moves back to the newly formed austenite.

In Fig. 10, the total energy dissipation in the both alloys is plotted together with available chemical driving force at the initial stage ($S_\gamma = 0.1$ μm) for the γ→α transformation at different temperatures. Again, due to the absence of Nb in solid solution in the transformed ferrite (i.e. newly formed austenite), the total dissipation for γ→α transformation in both alloys is deemed to be caused by Mn trapping at interface. Fig. 10a shows that at 750 °C, the chemical driving forces for both alloys cannot surpass the total dissipation at any interface velocity, thus the transformation is mainly controlled by the bulk diffusion of Mn in the austenite, which corresponds to the stagnant stage during the cooling process. When the temperature drops to the 729 °C (Fig. 10b), the chemical driving force of both alloys can overcome the dissipation caused by the Mn spike, which indicates the reaction has proceeded through the NPLE mode, thus yielding a visible expansion part from dilation curves. According to the same criterion for PF calculation as the α→γ transformation, the amount of PF for γ→α transformation is derived to be only 5 J/mol as indicated in Fig. 10b and corresponds to 2 °C supercooling in Fig. 9b. Hence, the PF for γ→α transformation is quite small in comparison to the chemical driving force, which is about 20 times larger.

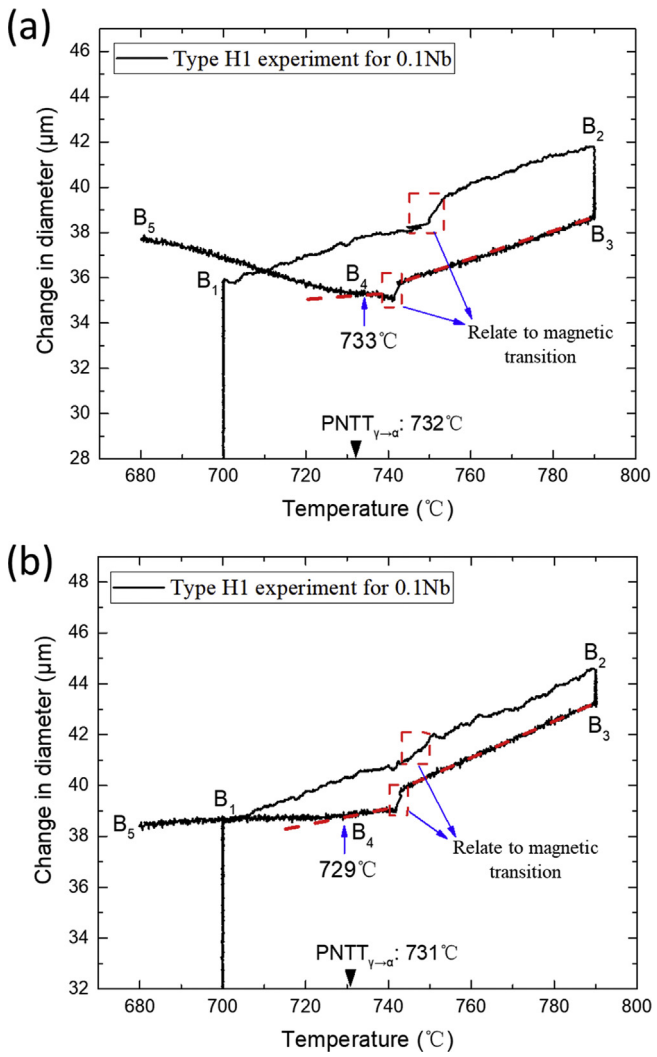

Fig. 9. The partial dilatation curves as a function of temperature for the (a) 0Nb and (b) 0.1Nb alloys during the type H1 experiment.

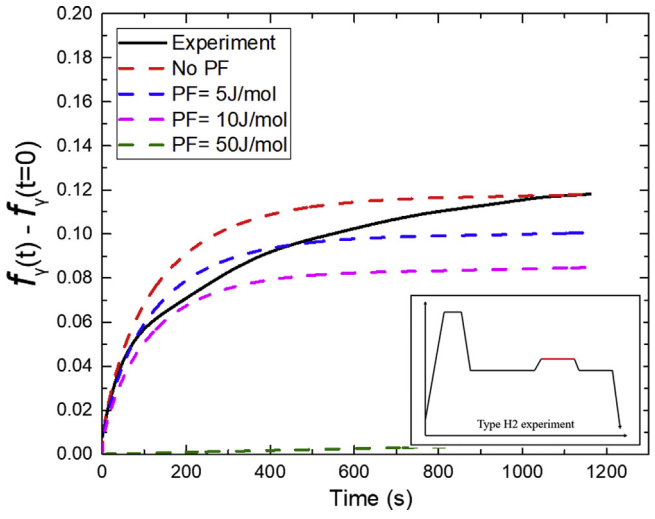

Fig. 8. The fraction of growing austenite predicted by the GEB model and measured by experiment as a function of time during the isothermal α→γ transformation at 790 °C in the 0.1Nb alloy.

Fig. 11 shows the fraction of ferrite predicted by the GEB model and measured by experiments as a function of time during the isothermal γ→α transformation at 700 °C in the 0.1Nb alloy. The vertical axis symbols of $f_\alpha(t=0)$ and $f_\alpha(t)$ represents the ferrite fraction at the initial stage and the certain time during isothermal process, respectively. Likewise, by considering different values of PF, the kinetics predicted by the GEB model can well fit the experimental result for a PF value in the range of 0–8 J/mol, which is consistent with the obtained value from the type H1 experiment. A large PF value such as 50 J/mol leads to a complete mismatch between the experiments and the calculations, and therefore is deemed unlikely.

4.2. Discussion

4.2.1. The accuracy of the values of PF

Fig. 12 shows the chemical driving force and the dissipation at zero interface velocity as a function of temperature during the partial cyclic transformations. For the case of continuous heating (Fig. 12a), the point A is the intersection of chemical driving force curve and the dissipation curve at zero velocity, which is the critical

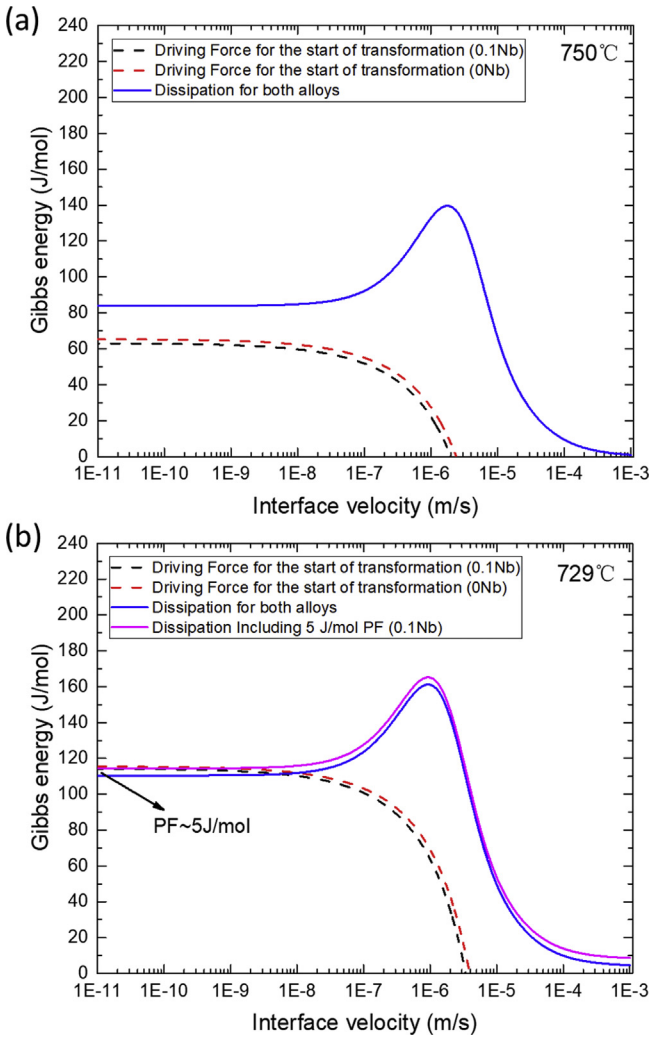

Fig. 10. The total energy dissipation and available chemical driving force at the initial stage ($S_\alpha = 0.1$ μm) for the both alloys during the $\gamma \rightarrow \alpha$ transformation at (a) 750 °C and (b) 729 °C, respectively.

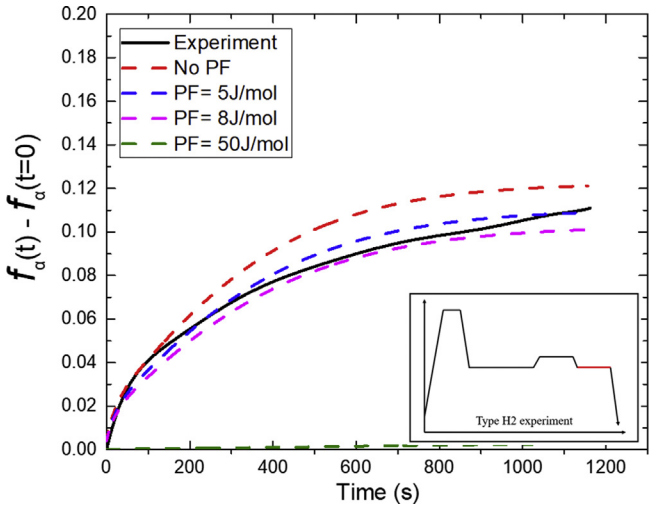

Fig. 11. The fraction of growing ferrite predicted by the GEB model and measured by experiments as a function of time during the isothermal $\gamma \rightarrow \alpha$ transformation at 700 °C in the 0.1Nb alloy.

temperature for the $\alpha \rightarrow \gamma$ transformation (i.e. $PNTT_{\alpha \rightarrow \gamma}$). However, due to the existence of PF (15 J/mol), the dissipation curve will move upward, and lead to a higher transformation starting temperature (point B). Likewise, as shown in Fig. 12b, the point C is $PNTT_{\gamma \rightarrow \alpha}$. Due to an additional 5 J/mol PF, the ferrite transformation starting temperature is decreased to point D. According to the above analysis, it can be concluded that the value of PF can be directly determined by the difference between PNTT and experimentally measured transformation starting temperature. Therefore, the accuracy of transformation starting temperature measured by experiments is directly linked to the derived PF. After several repetition of type I1 and type H1 experiments, the measured transformation starting temperatures were found to fluctuate within ±2 °C for both transformations, e.g. the PF vary within the range of 11–19 J/mol for the $\alpha \rightarrow \gamma$ transformation and 0–10 J/mol for the $\gamma \rightarrow \alpha$ transformation, respectively. Although the precise value of PF cannot be determined as a result of existing uncertainties, it is clear that the PF exerted by IPd carbides are quite small compared to chemical driving force, otherwise the stagnant stage with respect to PNTT will be easily detected and measured.

Actually, as shown in a recent work [36], the morphology of carbides is related to the α/γ interface orientation relationship (OR),

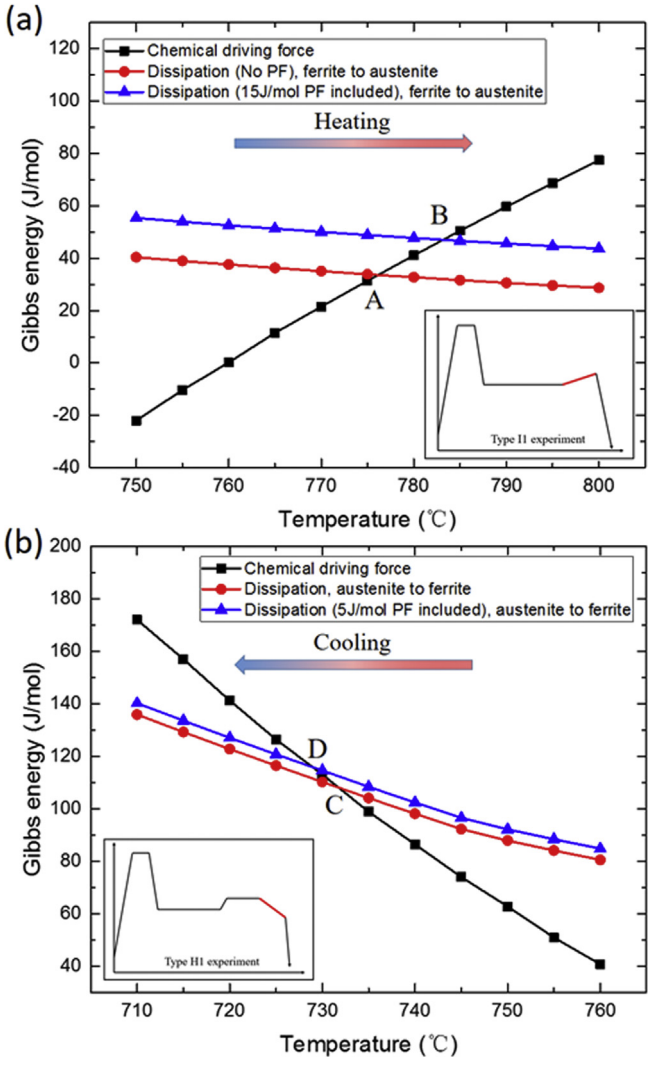

Fig. 12. The chemical driving force and dissipation at zero interface velocity as a function of temperature during the (a) $\alpha \rightarrow \gamma$ and (b) $\gamma \rightarrow \alpha$ transformations.

i.e. the VC interphase precipitation tends to be induced at the side of interfaces without K-S OR, while it could be significantly inhibited or even devoid behind the interfaces with K-S OR. Thus the effect of heterogeneity of IP on the PF obtained needs to be considered. Since the mobility of interface with non K-S OR is significantly larger than that with a K-S OR, it is believed that the visible deviation of dilation curves during cycling is mainly attributed to the ferrite (or austenite) growth via the migration of interfaces with non K-S OR, while the interfaces with K-S OR play a marginal role for the transformation initiation. Therefore, the PF derived from cyclic experiments is thought to be an overall parameter that mainly reflects the interaction between the non K-S OR interfaces and interphase precipitated carbides.

4.2.2. PF dependence on transformation directions

From a physical perspective, it should also be noted that the dependence of PF on the transformation direction might be caused by the following reasons: One is the interfacial coherency between carbides and matrix. Generally, the B1(NaCl)-type carbides tend to form the coherent (or semicoherent) interface and exhibit the Baker-Nutting orientation relationship (B-N OR) with the ferrite matrix [37,38], which leads to a lower interfacial energy. However, once the α/γ interface passed through the dispersion of coherent carbide arrays during $\alpha \rightarrow \gamma$ transformation (Fig. 1b(II)), the carbide-matrix interface would change from the coherency to the incoherency. Then the amount of PF is likely to vary when the α/γ interface migrates over these incoherent carbides during the subsequent $\gamma \rightarrow \alpha$ transformation (Fig. 1b(III)). Based on the theoretical study by Yang and Enomoto [39,40], the (001) interfacial energy of NbC/austenite with Cube-Cube OR (~3 J/m^2) is larger than that of NbC/ferrite with B-N OR (~1.8 J/m^2). Hence, the total energy of system will increase after the low-energy NbC/ferrite interfaces are replaced by the high energy incoherent ones, thus requiring larger driving force to initiate interface migration, i.e. the coherent carbides are more effective in pinning interfaces than the incoherent ones, which seems to be responsible for the relatively larger PF in $\alpha \rightarrow \gamma$ transformation than that in $\gamma \rightarrow \alpha$ transformation. Similar conclusions were also draw about GB-particle interaction based on the Zener's theory [5,41].

Secondly, the carbide arrays in the ferrite near the interface are possibly coarsening by boundary diffusion and bulk diffusion during the $\alpha \rightarrow \gamma$ transformation, which results in the decrease of PF when these carbides meet the α/γ interface again during the subsequent $\gamma \rightarrow \alpha$ transformation. In order to validate it, one may easily focus on the carbide distribution in austenite after second interrupted quenching in the type H2 cycle. However, as the austenite cannot be preserved at room temperature, it becomes challenging to directly observe the carbides in martensite due to the interference of high-density dislocations, and even dark field measurements do no work well for the quite weak diffraction spot of carbides near the interface. An indirect method to demonstrate the coarsening is that based on the type H1 specimen since (1) the carbides retained in austenite will be exposed into ferrite again when the interface moves back to austenite during final slow cooling, thus making the observation rather easier, (2) Owing to the short transformation period from 729^{0}C-680 °C (~5min), coarsening of the re-exposed carbide within the newly formed ferrite can be ignored, thus making the comparison more reasonable. Fig. 13 shows the carbide distribution near the α/γ interface after a type H1 cycle. The carbides, which are expected to have been exposed to a transformation from austenite into ferrite, grew obviously around the interface, and their size was measured to be about 9.4 ± 2.1 nm, i.e. more than 1.5 times bigger than it was. Similar results are also obtained in other regions containing α/γ interfaces. Hence, carbide coarsening during the $\alpha \rightarrow \gamma$ transformation is inferred to be another important reason for PF decrease.

The last one is the volume fraction of carbides. The NbC might be partially dissolved due to the higher isothermal temperature and the larger solubility of C and Nb in newly formed austenite compared with ferrite. However, according to thermodynamic calculations, the equilibrium volume fraction of NbC decreases quite slightly (0.116% → 0.113%) when the temperature rises from 700 °C to 790 °C, which qualitatively indicates that carbides can be hardly dissolved during the cyclic phase transformations, and thereby the change of the carbide volume fraction is not the main factor to cause PF difference.

4.2.3. Comparison with classical Zener pinning model

With relatively precise values for the PF established using the GEB concept for interface migration, it is appropriate to compare these values with those predicted by the classical Zener pinning model that has been widely applied to analyze the particle-GB interaction during recrystallization, i.e. in the absence of phase transformations. As mentioned in the introduction, several assumptions were made in the derivation of the original Zener pinning equation. In order to improve its applicability for industrial conditions, the classical equation has been modified by numerous attempts over the past seven decades [7]. In Table 3, several commonly used and accepted modified Zener expressions for the PF are listed, where f is the volume fraction of IPd carbides (0.11%, evaluated by Thermo-Calc), V_m is the mole volume of matrix (7×10^{-6} m^3/mol), σ is the interfacial energy of α/γ interface (here assuming 1.4 J/m^2 as an incoherent interphase boundary [42]), and r is the radius of NbC carbides (about 3 nm, obtained from TEM). By substituting the above data into each equation, the maximum dissipations due to PF are found to be vary within 2–22 J/mol, which is of the same order of magnitude as the values derived in the present work. It reveals the fact that the classical Zener theory still has promising potential for carbide-interface interaction analysis, which is not confined to the particle-GB interaction, even if some assumptions clearly deviate from reality.

In order to qualitatively elucidate the PF effects on recrystallization or grain growth, a rough estimate can be made as follows: the GB migration is essentially driven by boundary curvature:

$$\Delta\mu = V_m \gamma_b \left(\frac{1}{r_1} + \frac{1}{r_2} \right) \tag{11}$$

where γ_b is the interfacial energy of grain boundary, r_1 and r_2 are

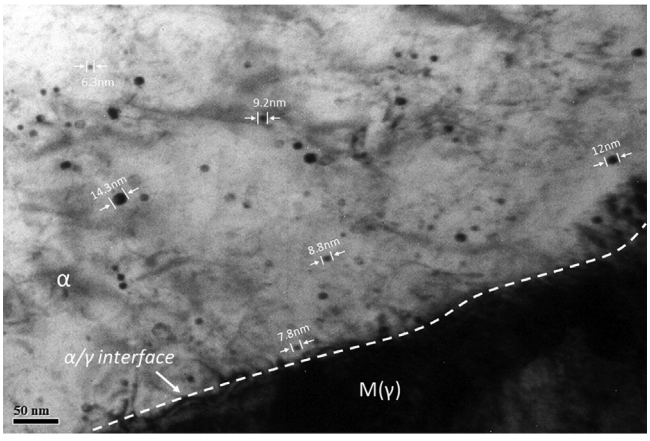

Fig. 13. TEM image showing carbide distribution near the α/γ interface after a type H1 cycle.

Table 3
The maximum dissipation due to PF calculated by the different modified Zener equations.

Reference	Equation (ΔG_z^{max} =)	Characteristics	Results (J/mol)
Zener [Smith] (1948) [2]	$3f\gamma V_m/4r$	Original equation, consider the surface density of particles on the GB as $3f/4\pi r^2$	2.71
Gladman (1966) [3] Nes et al. (1985) [5]	$3f\gamma V_m/2r$	Consider the surface density of particles on the GB as $3f/2\pi r^2$	5.39
Hazzledine et al. (1980) [43]	$9f\gamma V_m/8r$	Consider the obstacles as points and boundary bows out like the shape of spherical caps between pinning points	4.04
Doherty (1982) [41]	$6f\gamma V_m/r$	Consider the pinning effect of coherent particles on the GB	21.56
Nes et al. (1985) [5]	$1.3\gamma f^{0.92} V_m/r$	Consider a random distribution of particles on the GB	8.05
Hunderi et al. (1989) [44]	$0.33\gamma f^{0.87} V_m/r$	Consider the Louat effect [45], i.e., the particles ahead of the GB can attract the boundary and assist its movement	2.87

the principal radius of boundary curvature. For simplicity, the grain shape is assumed as spherical. By choosing $\gamma_b \sim 1.0\,J/m^2$ and $r_1 = r_2 \sim 10\,\mu m$ in a typical metal system, the resulted driving force is about 1.4 J/mol, which is quite comparable with the derived PF. Therefore, the pinning effect imposed by the fine dispersed particles cannot be ignored for the passage of grain boundaries during recrystallization. Nevertheless, in the case of the general phase transformation (i.e. 100% parent phase → 100% new phase), the effect of interface pinning will be different. The kinetics of the first $\gamma \rightarrow \alpha$ transformation at 700 °C for the 0.1Nb alloy are simulated by the GEB model and is plotted in Fig. 14. The figure indicates that with the addition of PF, the reaction gradually slows down but not very obviously, which can be expressed as an increasing lag time for entering the transformation stasis (see inset, t_{PF} and t_0 in the left vertical axis represent the start time of the transformation stasis with consideration of PF and no PF). The ferrite fraction at transformation stasis decreases only marginally, such that it can be deemed as constant (see the right vertical axis of inset). The main reason for the above result is that the values of PF are usually much smaller than the chemical driving force for solid-state phase transformations, thus leading to a marginal effect on the interface migration. It also explains why the PF induced transformation retardation cannot be easily detected in single transformation experiments.

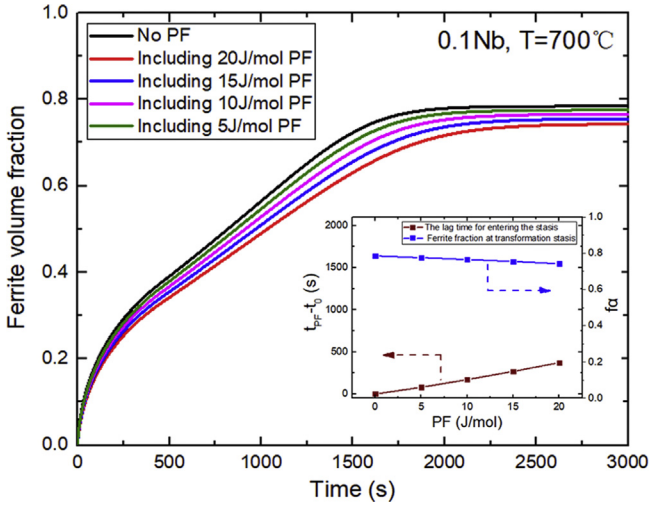

Fig. 14. The kinetics of the first $\gamma \rightarrow \alpha$ transformation at 700 °C in the 0.1Nb alloy simulated by the GEB model. Inset summarizes the stasis ferrite fractions and the lag time for entering the transformation stasis predicted by the GEB model as a function of PF.

5. Conclusion

Cyclic phase transformation experiments on two model alloys 0.1%C-1.5%Mn without or with 0.1%Nb (all percentages are by weight) combined with the GEB model have been applied to study the interaction between the moving α/γ interfaces and IPd carbides. The following conclusions can be drawn:

1) Based on the type I1 and type H1 experimental results, the delayed critical transformation temperature is attributed to the PF exerted by IPd carbides. The estimated values of PF is about 15 J/mol for the $\alpha \rightarrow \gamma$ transformation and about 5 J/mol for the $\gamma \rightarrow \alpha$ transformation, respectively. The range of PF derived from type H2 experiment gives a consistent result with above values.
2) The amount of PF is essentially related to the length of stagnant stage with respect to the PNTT, which can be affected by the existing errors in measurement of transformation starting temperature. Relatively smaller PF in $\gamma \rightarrow \alpha$ transformation than that in $\alpha \rightarrow \gamma$ transformation are presumably due to the coherency change of carbide-matrix interface and carbide coarsening during cycling.
3) The PF predicted by the different modified Zener equations are at the same order of magnitude as that of this work, which indicates the classical Zener theory still has promising potential for carbide-interface interaction analysis. A rough analysis indicates that PF can play a significant role on the recrystallization process as its value is comparable to the driving force for GB migration, while the influence of PF on the phase transformation kinetics can (to a first order) be ignored, due to its value being quite small compared to the chemical driving force.

Acknowledgements

H.K. Dong and H. Chen are thankful to Dr. Hung-Wei Yen for several experiments discussion. Z G. Yang acknowledges financial support from the National Natural Science Foundation of China (Grant 51771100). H. Chen acknowledges financial support from Beijing Natural Science Foundation(2182024), the National Natural Science Foundation of China (Grant 51501099), National Key R&D program of China (2016YFB0300104) and National Young 1000-Talents Program (D1101073). C. Zhang acknowledges financial support from the National Natural Science Foundation of China (Grant 2015CB654802), the National Magnetic Confinement Fusion Energy Research Project of China (Grant 2015GB118001) and Fund of Key Laboratory of Advanced Materials of Ministry of Education (Grant 2017AML09). S. van der Zwaag acknowledges receiving a 1000-talent grant from the Chinese government in the context of the Recruitment program for Foreign Experts (7th cohort).

References

[1] T. Gladman, The Physical Metallurgy of Microalloyed Steels, Maney Publishing, 2002.
[2] C.S. Smith, Grains, phases, and interphases: an interpretation of microstructure, Trans. Metall. Soc. A.I.M.E. 175 (1948) 15–51.
[3] T. Gladman, On the theory of the effect of precipitate particles on grain growth in metals, Proc. Roy. Soc. Lond. 294 (1966) 298–309.
[4] M. Ashby, J. Harper, J. Lewis, The interaction of crystal boundaries with second-phase particles, Trans. Metall. Soc. A.I.M.E. 245 (1969) 413–420.
[5] E. Nes, N. Ryum, O. Hunderi, On the Zener drag, Acta Metall. 33 (1985) 11–22.
[6] P.R. Rios, Overview no. 62: a theory for grain boundary pinning by particles, Acta Metall. 35 (1987) 2805–2814.
[7] P.A. Manohar, M. Ferry, T. Chandra, Five decades of the Zener equation, ISIJ Int. 38 (1998) 913–924.
[8] N. Wang, Y. Ji, Y. Wang, Y. Wen, L.-Q. Chen, Two modes of grain boundary pinning by coherent precipitates, Acta Mater. 135 (2017) 226–232.
[9] A.T. Davenport, R.W.K. Honeycombe, Precipitation of carbides at $\gamma \rightarrow \alpha$ boundaries in alloy steels, Proc. Roy. Soc. Lond. 322 (1971) 191–205.
[10] R.W.K. Honeycombe, R.F. Mehl, Transformation from austenite in alloy steels, Metall Trans A – Phys Metall Mater Sci. 7 (1976) 915–936.
[11] P. Li, J.A. Todd, Application of a new model to the interphase precipitation reaction in vanadium steels, Metall. Mater. Trans. 19 (1988) 2139–2151.
[12] R. Lagneborg, S. Zajac, A model for interphase precipitation in V-microalloyed structural steels, Metall Mater Trans A - Phys Metall Mater Sci. 32 (2001) 39–50.
[13] R. Okamoto, J. Ågren, A model for interphase precipitation based on finite interface solute drag theory, Acta Mater. 58 (2010) 4791–4803.
[14] M.Y. Chen, M. Gouné, M. Verdier, Y. Bréchet, J.R. Yang, Interphase precipitation in vanadium-alloyed steels: strengthening contribution and morphological variability with austenite to ferrite transformation, Acta Mater. 64 (2014) 78–92.
[15] H.-W. Yen, P.-Y. Chen, C.-Y. Huang, J.-R. Yang, Interphase precipitation of nanometer-sized carbides in a titanium–molybdenum-bearing low-carbon steel, Acta Mater. 59 (2011) 6264–6274.
[16] R.A. Ricks, P.R. Howell, Bowing mechanism for interphase boundary migration in alloy steels, Met. Sci. 16 (1982) 317–322.
[17] R.A. Ricks, P.R. Howell, The formation of discrete precipitate dispersions on mobile interphase boundaries in iron-base alloys, Acta Metall. 31 (1983) 853–861.
[18] W.J. Liu, Computer simulation of VC precipitation at moving γ/α interfaces, Metall Mater Trans A - Phys Metall Mater Sci. 24 (1993) 2195–2207.
[19] M.Y. Chen, M. Gouné, M. Militzer, Y. Bréchet, J.-R. Yang, Superledge model for interphase precipitation during austenite-to-ferrite transformation, Metall. Mater. Trans. 45 (2014) 5351–5361.
[20] T. Murakami, H. Hatano, G. Miyamoto, T. Furuhara, Effects of ferrite growth rate on interphase boundary precipitation in V microalloyed steels, ISIJ Int. 52 (2012) 616–625.
[21] S. Mukherjee, I.B. Timokhina, C. Zhu, S.P. Ringer, P.D. Hodgson, Three-dimensional atom probe microscopy study of interphase precipitation and nanoclusters in thermomechanically treated titanium–molybdenum steels, Acta Mater. 61 (2013) 2521–2530.
[22] S. Mukherjee, I.B. Timokhina, C. Zhu, S.P. Ringer, P.D. Hodgson, Clustering and precipitation processes in a ferritic titanium-molybdenum microalloyed steel, J. Alloy. Comp. 690 (2017) 621–632.
[23] H. Chen, S. van der Zwaag, Application of the cyclic phase transformation concept for investigating growth kinetics of solid-state partitioning phase transformations, Comput. Mater. Sci. 49 (2010) 801–813.
[24] H. Chen, B. Appolaire, S. van der Zwaag, Application of cyclic partial phase transformations for identifying kinetic transitions during solid-state phase transformations: experiments and modeling, Acta Mater. 59 (2011) 6751–6760.
[25] Z.B. Dai, R. Ding, Z.G. Yang, C. Zhang, H. Chen, Elucidating the effect of Mn partitioning on interface migration and carbon partitioning during Quenching and Partitioning of the Fe-C-Mn-Si steels: modeling and experiments, Acta Mater. 144 (2018) 666–678.
[26] G. Miyamoto, K. Shinbo, T. Furuhara, Quantitative measurement of carbon content in Fe–C binary alloys by atom probe tomography, Scripta Mater. 67 (2012) 999–1002.
[27] H. Chen, S. van der Zwaag, A general mixed-mode model for the austenite-to-ferrite transformation kinetics in Fe–C–M alloys, Acta Mater. 72 (2014) 1–12.
[28] D.E. Coates, Diffusion-controlled precipitate growth in ternary systems I, Metall. Trans. 3 (1972) 1203–1212.
[29] D.E. Coates, Diffusion controlled precipitate growth in ternary systems: II, Metall. Trans. 4 (1973) 1077–1086.
[30] H. Chen, S. van der Zwaag, Modeling of soft impingement effect during solid-state partitioning phase transformations in binary alloys, J. Mater. Sci. 46 (2011) 1328–1336.
[31] G. Purdy, Y. Brechet, A solute drag treatment of the effects of alloying elements on the rate of the proeutectoid ferrite transformation in steels, Acta Metall. 43 (1995) 3763–3774.
[32] M. Hillert, L. Höglund, Mobility of α/γ phase interfaces in Fe alloys, Scripta Mater. 54 (2006) 1259–1263.
[33] J. Park, M. Jung, Y.K. Lee, Abnormal expansion during the ferro- to paramagnetic transition in pure iron, J. Magn. Magn Mater. 377 (2015) 193–196.
[34] H. Chen, K. Zhu, L. Zhao, S. van der Zwaag, Analysis of transformation stasis during the isothermal bainitic ferrite formation in Fe–C–Mn and Fe–C–Mn–Si alloys, Acta Mater. 61 (2013) 5458–5468.
[35] J. Fridberg, L.-E. Torndahl, M. Hillert, Diffusion in iron, Jernkontorets Ann. 153 (1969) 263–276.
[36] Y.J. Zhang, G. Miyamoto, K. Shinbo, T. Furuhara, Effects of α/γ orientation relationship on VC interphase precipitation in low-carbon steels, Scripta Mater. 69 (2013) 17–20.
[37] D.P. Dunne, R.M. Smith, Structural aspects of alloy carbonitride precipitation in microalloyed steels, Mater. Forum 11 (1988) 166–181.
[38] R.G. Baker, J. Nutting, Precipitation processes in steels, Iron and Steel Institute, Special Report 64 (1959).
[39] Z.G. Yang, M. Enomoto, Calculation of the interfacial energy of B1-type carbides and nitrides with austenite, Metall. Mater. Trans. 32 (2001) 267–274.
[40] Z.G. Yang, M. Enomoto, Discrete lattice plane analysis of Baker-Nutting related B1 compound/ferrite interfacial energy, Mater. Sci. Eng. 332 (2002) 184–192.
[41] R.D. Doherty, Role of interfaces in kinetics of internal shape changes, Met. Sci. J 16 (1982) 1–14.
[42] H. Song, J.J. Hoyt, A molecular dynamics study of heterogeneous nucleation at grain boundaries during solid-state phase transformations, Comput. Mater. Sci. 117 (2016) 151–163.
[43] P.M. Hazzledine, P.B. Hirsch, N. Louat, in: N. Hansen, et al. (Eds.), Proc, Ist Int.Symp. on Metallurgy and Materials Science, Riso National Laboratory, Roskilde, Denmark, 1980, p. 159.
[44] O. Hundert, E. Nes, N. Ryum, On the zener drag—Addendum, Acta Metall. 37 (1989) 129–133.
[45] N. Louat, The resistance to normal grain growth from a dispersion of spherical particles, Acta Metall. 30 (1982) 1291–1294.